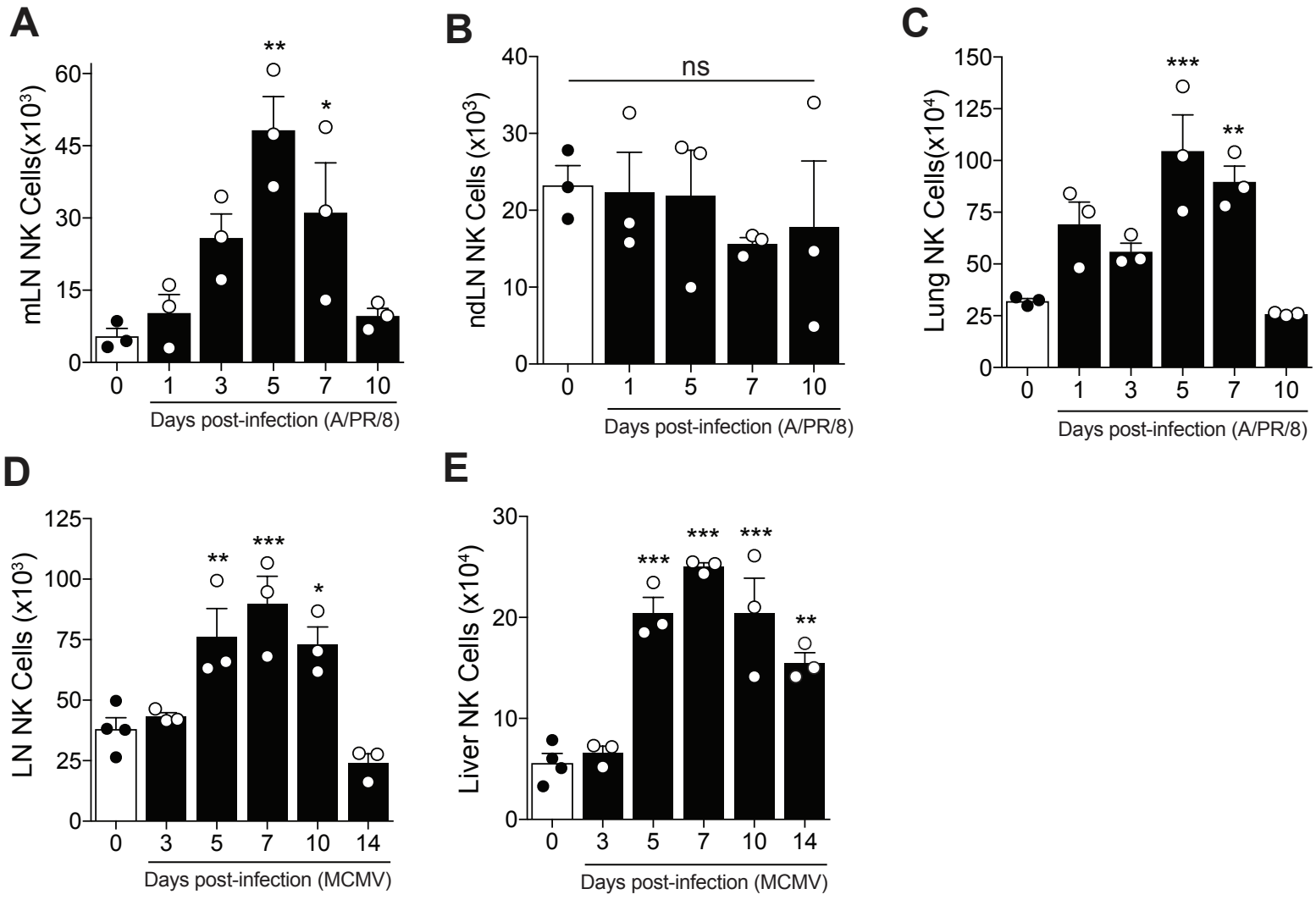

Supplementary Figure 1. Trafficking of NK cells to priming and target tissues throughout the course of viral infection. (**A-E**) Time course of absolute numbers of NK cells (CD3-NK1.1+) in the mediastinal lymph nodes (mLN) (**A**), non-draining lymph nodes (ndLN) (**B**), lung (**C**), draining lymph nodes (DLN) (**D**), and liver (**E**), of C57BL/6 at different time points post-APR8 (**A-C**) or post-MCMV (**D,E**) infection. Control (white-filled bars) mice were mock-infected by receiving either 40 µL of PBS (APR8 control) i.n. or 0.2 mL of RPMI (MCMV control) i.p., whereas infected mice (black-filled bars) were either infected with 20 PFU APR8 in 40 µL of PBS i.n. or 5 x 10^3 PFU MCMV in 0.2 mL of RPMI i.p. n=3 or 4 mice per group representative of 2-3 experiments. One-way ANOVA with Tukey post-test used to compare groups. * $p<0.05$, ** $p<0.01$, *** $p<0.001$.

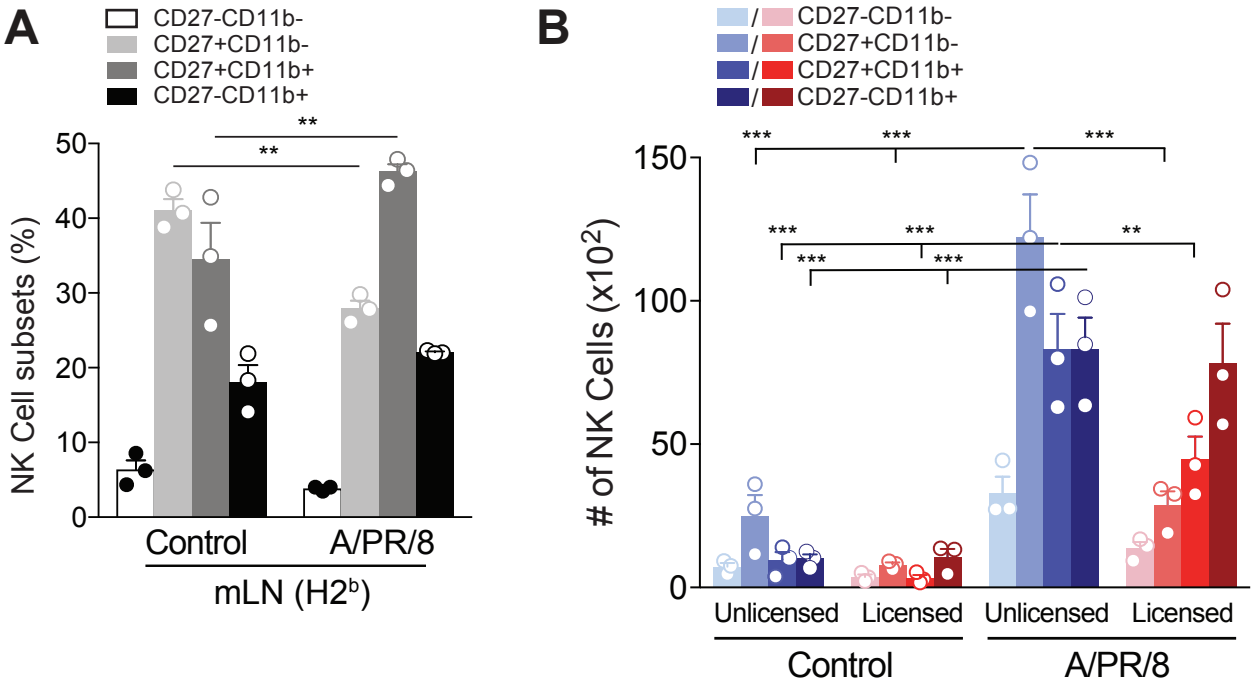

Supplementary Figure 2. Trafficking of NK cells to priming and target tissues throughout the course of viral infection. (**A**) Frequency of immature (CD27-CD11b-, CD27+CD11b-) and mature (CD27+CD11b+, CD27-CD11b+) NK cells in the mediastinal lymph nodes (mLN) of C57BL/6 (H2b) mice on day 5 post-APR8 infection. (**B**) Absolute number of immature and mature unlicensed and licensed NK cell subsets in the mLN of C57BL/6 (H2b) mice on day 5 post-APR8 infection. n=3 mice per group representative of 2-3 experiments. Two-way ANOVA with Tukey post-test used to compare groups. ** $p<0.01$, ***$p<0.001$.

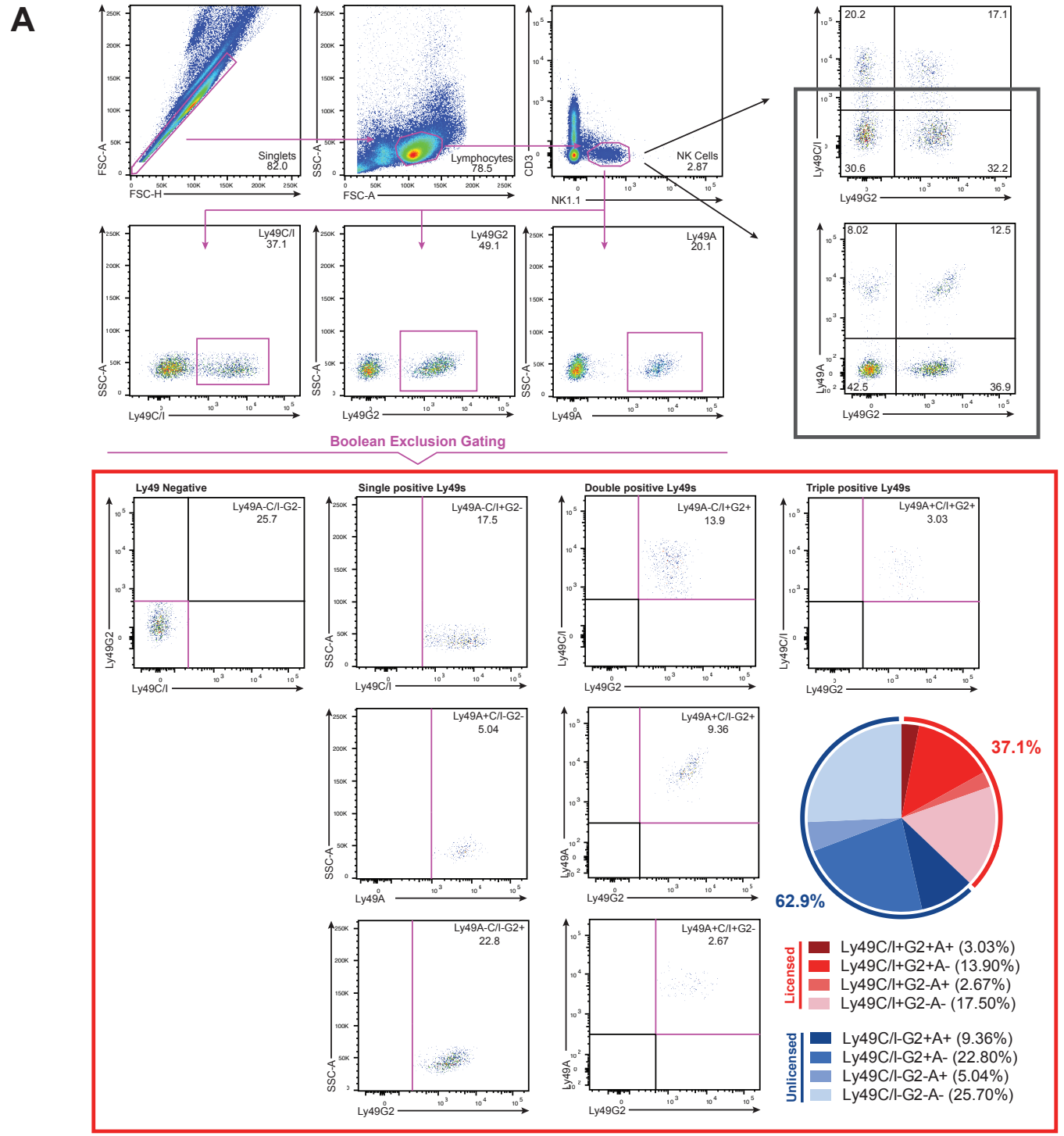

B

Receptor	Binds to	C57BL/6 ($H2^b$)	B10.D2 ($H2^d$)
Ly49C/I	$H2^b$	Licensed	Unlicensed
Ly49G2	$H2^d$	Unlicensed	Licensed
Ly49A	$H2^d$	Unlicensed	Licensed

Receptor	Binds to	C57BL/6 ($H2^b$)	B10.D2 ($H2^d$)
Ly49C/I+G2+A+	$H2^b$, $H2^d$	Licensed	Licensed
Ly49C/I+G2+A-	$H2^b$, $H2^d$	Licensed	Licensed
Ly49C/I+G2-A+	$H2^b$, $H2^d$	Licensed	Licensed
Ly49C/I+G2-A-	$H2^b$	Licensed	Unlicensed
Ly49C/I-G2+A+	$H2^d$	Unlicensed	Licensed
Ly49C/I-G2+A-	$H2^d$	Unlicensed	Licensed
Ly49C/I-G2-A+	$H2^d$	Unlicensed	Licensed
Ly49C/I-G2-A-	-	Unlicensed	Unlicensed

Supplementary Figure 3. Comparison between boolean gating and conventional gating to determine the phenotype of NK cell subsets. (**A**) Representative gating strategy comparing boolean gating (red square) and conventional gating (grey square) to identify Ly49-receptor subsets by staining for Ly49A, -G2, and –C/I on splenocytes from C57BL/6 mice. Boolean gating (red square) allows for the simultaneous identification of Ly49-negative, single-positive, double-positive, and triple-positive Ly49-expressing NK cell subsets, whereas conventional gating allows for pairwise comparisons of Ly49 receptors. Boolean gating allows for the identification and quanitification of CD3-NK1.1+Ly49C/I+G2+A+,

Supplementary Figure 3 continued. Ly49C/I+G2+A-, Ly49C/I+G2-A+, Ly49C/I+G2-A-, Ly49C/I-G2+A+, Ly49C/I-G2+A-, Ly49C/I-G2-A+, and Ly49C/I-G2-A- NK cell subsets, represented as percentages of each subset among total NK cells in the pie chart (bottom). (**B**) Classification of “licensed” and “unlicensed” NK cell subsets in C57BL/6 (H2b) and B10.D2 (H2d) mice based on the ability of specified Ly49 receptors to bind MHC class I molecules using either conventional gating (grey square) or Boolean gating (red square).

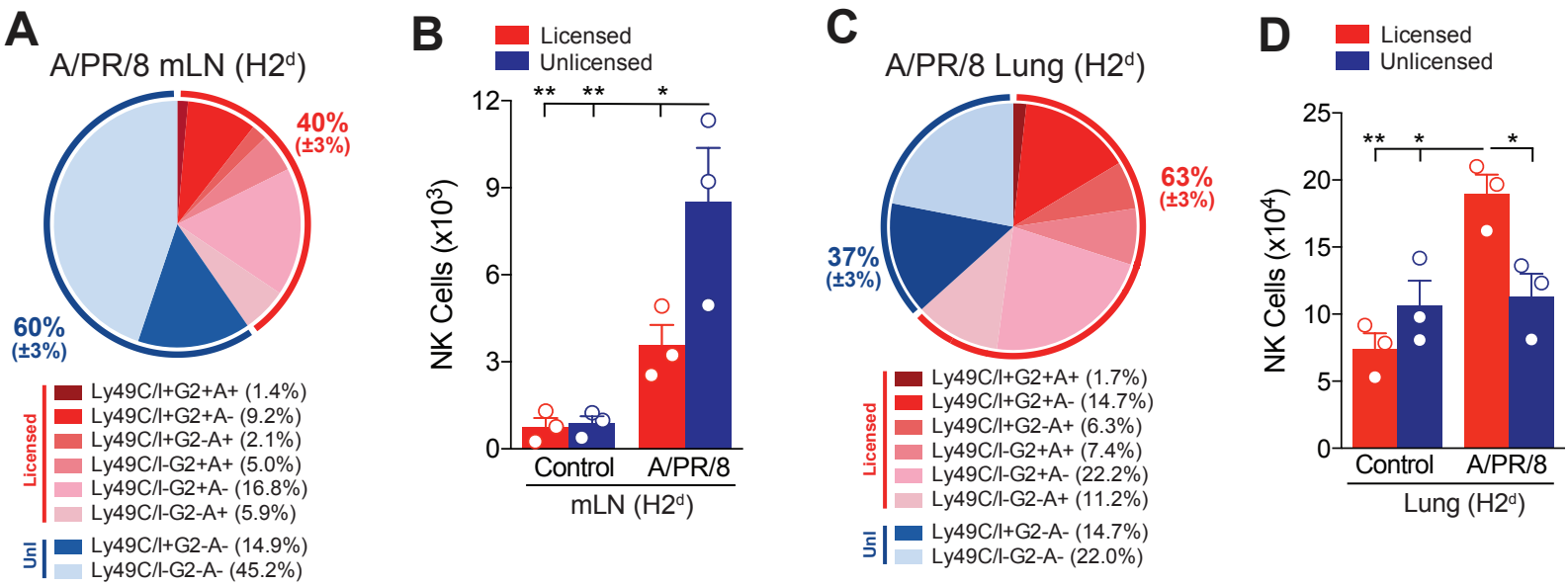

Supplementary Figure 4. B10.D2 NK subsets show similar licensing distribution patterns following viral infection. (**A**) Frequency or (**B**) absolute number of licensed (CD3-NK1.1+Ly49C/I+G2+A+, Ly49C/I+G2+A-, Ly49C/I+G2-A+, Ly49C/I-G2+A+, Ly49C/I-G2+A-, or Ly49C/I-G2-A+; shades of red) and unlicensed (CD3-NK1.1+Ly49C/I+G2-A-, or Ly49C/I-G2-A-; shades of blue) NK cell subsets in the mediastinal lymph nodes (mLN) of B10.D2 (H2d) mice on day 5 post-APR8 infection. (**C**) Frequency or (**D**) absolute number of licensed (shades of red) and unlicensed (shades of blue) NK cell subsets in the lung of B10.D2 (H2d) mice on day 5 post-APR8 infection. n=3 mice per group representative of 2-3 experiments. (**B,D**) Two-way ANOVA with Tukey post-test used to compare groups.

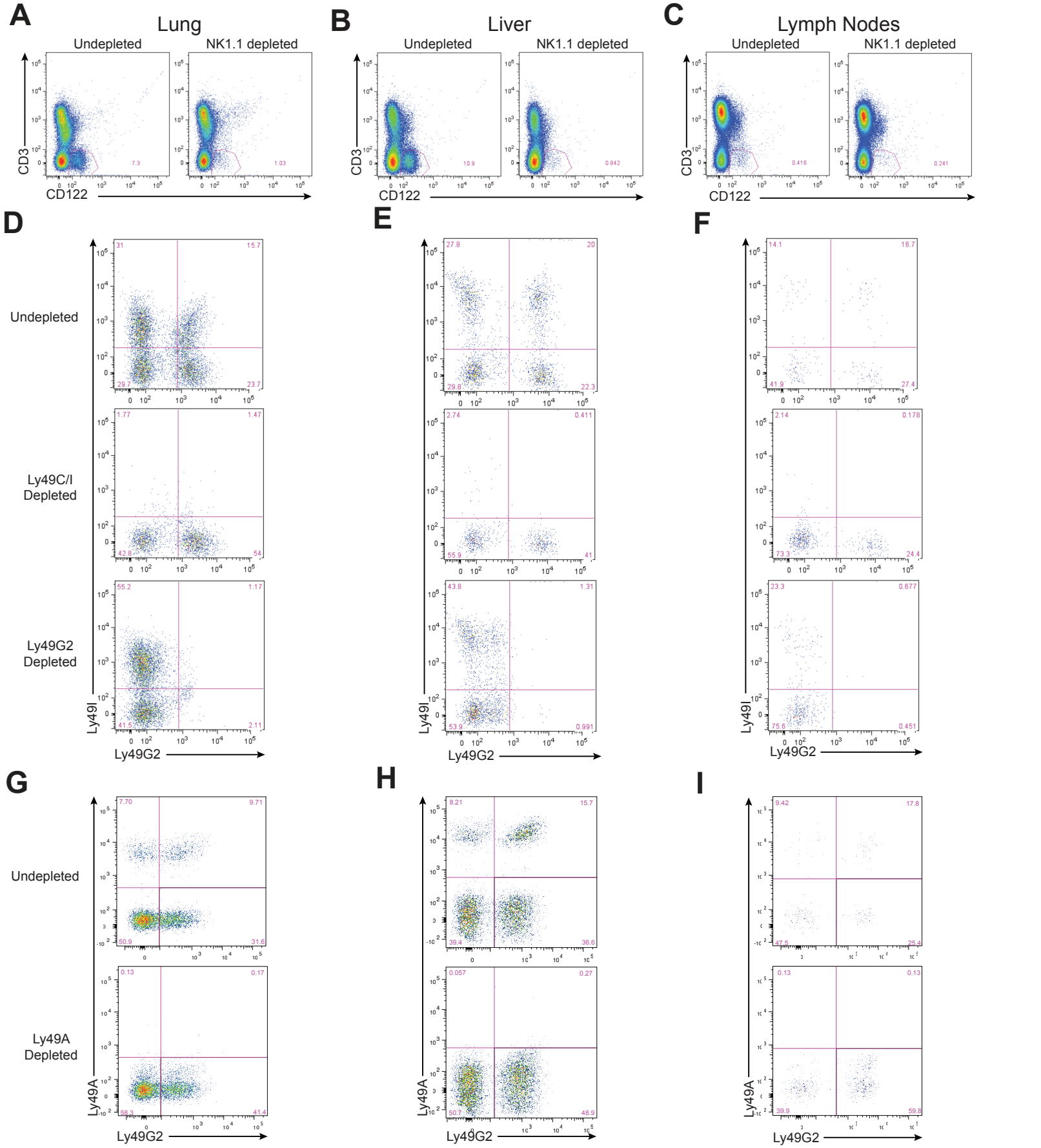

Supplementary Figure 5. Verification of successful depletion of specific NK populations with in vivo monoclonal antibody depletion in C57BL/6 mice. (**A-C**) non-depleted mIgG (left) and NK1.1 (PK136) (right) depleted C57BL/6 mice had lungs (**A**), livers (**B**), and lymph nodes (**C**) stained for CD3 and CD122. (**D-F**) Mice were either administered mouse/rat IgG (top) or given either anti-Ly49C/I (5E6) (middle) or anti-Ly49G2 (4D11) (bottom) and lungs (**D**), livers (**E**), and lymph nodes (**F**) were removed and stained for CD3-NK1.1+ and Ly49G2 (clone Cwy3) vs Ly49I (clone YLI-90). (**G-I**) Mice were either administered rat IgG (top) or given anti-Ly49A (YE1/32) (bottom) and lungs (**G**), livers (**H**), and lymph nodes (**I**) were removed and stained for CD3-NK1.1+ and Ly49G2 (clone 4D11) vs Ly49A (clone YE1/48.10.6). 300 µg of rIgG, anti-NK1.1, anti-Ly49G2, anti-Ly49C/I, or anti-Ly49A in 0.2 ml of PBS i.p. was given 2 days prior to infections. Flow plots are representative of 3 mice from 3 separate experiments.

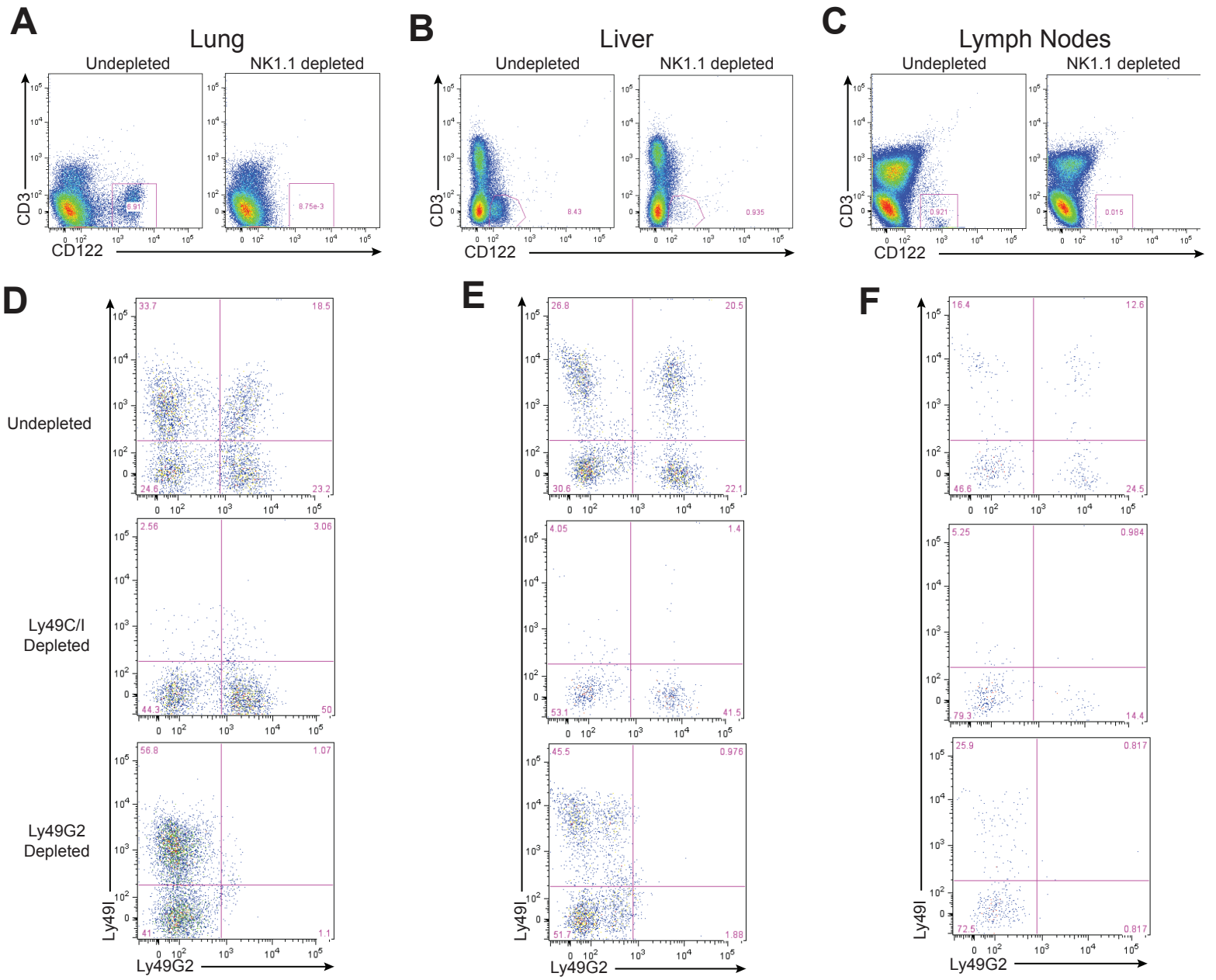

Supplementary Figure 6: Verification of successful depletion of specific NK populations with in vivo monoclonal antibody depletion in B10.D2 mice. (**A-C**) non-depleted mIgG (left) and NK1.1 (PK136) (right) depleted B10.D2 mice had lungs (**A**), livers (**B**), and lymph nodes (**C**) stained for CD3 and CD122. (**D-F**) Mice were either administered mouse/rat IgG (top) or given either anti-Ly49C/I (5E6) (middle) or anti-Ly49G2 (4D11) (bottom) and lungs (**D**), livers (**E**), and lymph nodes (**F**) were removed and stained for CD3-NK1.1+ and Ly49G2 (clone Cwy3) vs Ly49I (clone YLI-90). 300 µg of rIgG, anti-NK1.1, anti-Ly49G2, or anti-Ly49C/I in 0.2 ml of PBS I.P. was given 2 days prior to infections. Flow plots are representative of 3 mice from 3 separate experiments.

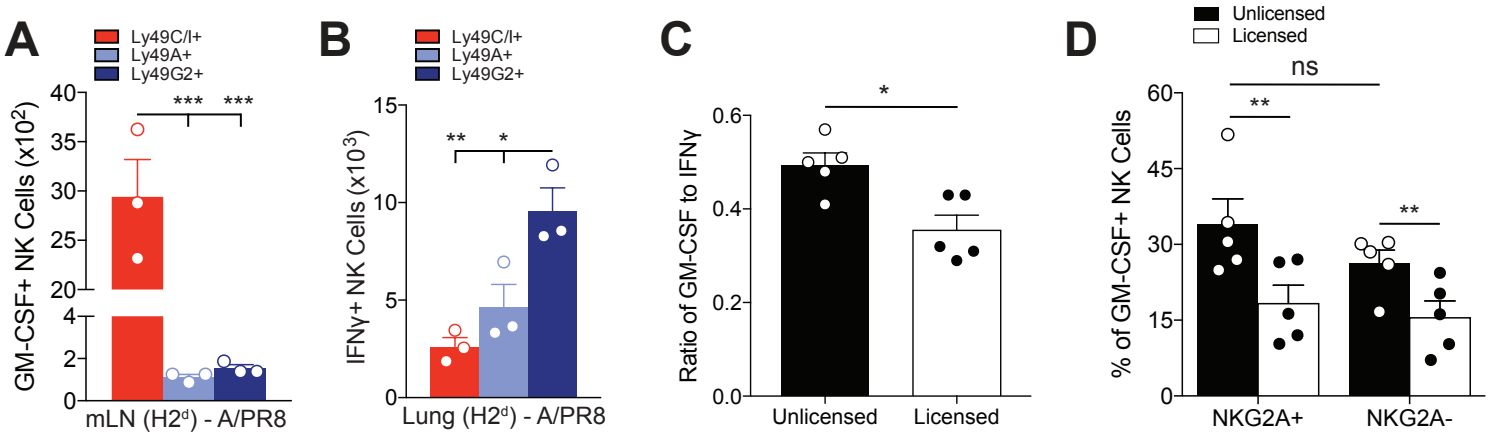

Supplementary Figure 7. B10.D2 and human NK subsets display cytokine profiles consistent with licensing. (**A**) Absolute number of NK cells that are GM-CSF+ and either CD3-NK1.1+Ly49G2+, Ly49A+, or Ly49C/I+ at day 5 after APR8 infection in the mediastinal lymph nodes (mLN) of B10.D2 mice. (**B**) Absolute number of NK cells that are IFN-γ+ and either CD3-NK1.1+Ly49G2+, Ly49A+, or Ly49C/I+ at day 5 after APR8 infection in the lung of B10.D2. (**C**) Aggregate ratio of GM-CSF to IFN-γ production by unlicensed and licensed NK cells. (**D**) Percentage of NKG2A+ or NKG2A- among either licensed or unlicensed NK cell populations that are GM-CSF+ after 16 hours of PMA/Ionomycin stimulation. Murine data: n=3 mice per group representative of 2-3 experiments. One-way ANOVA with Tukey post-test used to compare groups. Human data: Experiments were performed in duplicates; 1-3 aggregated single-positive NK cell subsets per unlicensed or licensed group. Five distinct individuals were used to obtain NK cells from PBMCs. * $p<0.05$, ** $p<0.01$, *** $p<0.001$.

SUPPLEMENTAL EXPERIMENTAL PROCEDURES

Cell Preparation and Flow Cytometry

Recipient mice were sacrificed at different time points post-infection. Single cell suspensions were prepared from the harvested livers, lungs, and lymph nodes (for influenza A/PR/8 studies: draining lymph nodes included mediastinal lymph nodes and non-draining lymph nodes included brachial, axillary, and inguinal lymph nodes; for MCMV studies: draining lymph nodes included brachial, axillary, inguinal and submandibular lymph nodes as it is a diffuse viral infection) in PBS with 1% FBS. Cells were then incubated with Fc block 2.4G2 mAb to block nonspecific binding and then stained with varying combinations of indicated fluorochrome-conjugated mAbs (antibodies used listed below). Isotype matched rat/mouse IgG mAbs were used as negative staining controls. Intracellular staining was performed using the BD Cytofix/Cytoperm Fixation/Permeabilization kit (BD, San Jose, CA). Cells were incubated for four hours at 37 degrees C with 1μl/mL Golgiplug, 1μl/mL Golgistop, 50ng/mL phorbol 12-myristate 13-acetate (PMA), and 1μg/mL ionomycin prior to surface staining. Cells were then permeabilized with the BD Fixation/Permeabilization solution following manufacturer instructions.

The following fluorochrome-conjugated mAbs were purchased from BioLegend (San Diego, CA): Pacific Blue PB-anti-CD45 (30-F11), anti-CD90.2 (Thy1.2; 30-H12), alexa fluor 647-AF-anti-NK1.1 (PK136), Biotin-anti-Ly49H (3D10), Cyanine 5-cytidine 3’5’bisphospate PCPCy5-strepavadin, phycoerythrin PE-Cy7-anti-CD3 (145-2C11), PE-anti-Ly49A (YE1/48.10.6), BV785-anti-CD3 (17A2), BV421-anti-CXCR3 (CXCR3-173), BV605-anti-CD86 (GL-1), APC/Cy7-anti-I-A/I-E (M5/114.15.2), BV711-anti-CD4 (GK1.5), BV711-anti-CD4 (RM4-5), BV605-anti-CD8a (53-6.7), anti-CD11c (N418), and APC-anti-CD122 (TM-β1). From Becton Dickson (BD) Pharmingen (San Jose, CA): fluorescein isothiocyanate (FITC)-anti-Ly49G2 (4D11), anti-Ly49G2 (Cwy3), anti-CD8a (53-6.7), anti-CD19 (1D3), and anti-NKG2A (20d5), PE-anti-Ly49C/I

(5E6), anti-Ly49I (YLI-90), anti-CXCR3 (CXCR3-173), anti-IFNγ, anti-GM-CSF, rIgG, APC-Cy7-anti-CD25 (PC61), anti-Ly49A (A1), and CD32+CD16 antibody (2.4G2) to block FCgII/III receptor-mediated nonspecific binding. From eBioscience (San Diego, CA): anti-MHC class II (M5/114.15.2), and anti-CD4 (L3T4), PE-eFluor610-anti-NK1.1 (PK136), PerCP-eFluor710-anti-Ly49G2 (4D11), and PE/Cy7-anti-IFNg (XMG1.2).

Human conjugated antibodies included : APC-eFluor 780-conjugated anti-CD3 (clone SK7, eBioscience, San Diego, CA), Brilliant Violet 605-conjugated anti-CD56 (clone HCD56, BioLegend, San Diego, CA), FITC-conjugated anti-KIR2DL1 (clone 143211, R&D Minneapolis, MN); Alex fluor 700-conjugated anti-KIR3DL1 (clone DX9, BioLegend, San Diego, CA); PE-cy7-conjugated anti-KIR2DL2/L3/S2 (clone GL183, Beckman Coulter, Brea, CA); APC-conjugated anti-NKG2A (clone Z199, Beckman Coulter, Brea, CA), V450-conjugated anti-IFN-y (B27, BD Bioscience, Chicago, IL); PE-conjugated anti-IL22 (clone BG/IL22, Biolegend, , San Diego, CA), and Pacific Blue-conjugated anti-GM-CSF (clone BVD2-21C11, Biolegend, San Diego, CA).

Tetramers were provided by the NIH Tetramer Core Facility (Emory University, Atlanta, GA). MCMV MHC class I tetramers: H-2D^{b} MHC allele with M45$_{985-993}$ epitope, H-2L^{d} with IE-1$_{168-176}$ epitope, and H-2D^{d} with m164$_{257-265}$ epitope. Influenza MHC class I tetramers: H-2D^{b} with NP$_{366-374}$ epitope, H-2K^{d} with NP$_{147-155}$ epitope. All tetramers were conjugated with an APC, PE, or AF488 fluorphore.

Microarray analysis

Microarray probe intensity values (CEL files) were background-corrected, summarized, and normalized using the Robust Multi-array Average (RMA16) algorithm(1) and filtered for raw signal intensity values in the range of the 20th-100th percentile (lowe/upper cut-off). Comparison analysis was performed to identify genes that were differentially expressed (≥1.25-fold) between the different NK cell subsets (Ly49-negative, Ly49G2/A+, and Ly49C/I+).

Biological interpretation of the resulting lists of differentiallly expressed genes was performed using the functional annotation and clustering tools available at the Database for Annotation, Visualization and Integrated Discovery (DAVID) Bioinformatics Resources 6.7(2, 3) to reveal enrichment for gene ontology and pathway annotations based upon gene-gene functional relationships with *kappa* statistics(4), a novel agglomeration algorithm to organize genes into biological modules, and then to calculate enrichment scores based on a Fisher Exact Test(5).

References

1. Irizarry RA, Wang C, Zhou Y, and Speed TP. Gene set enrichment analysis made simple. *Statistical methods in medical research.* 2009;18(6):565-75.
2. Huang da W, Sherman BT, and Lempicki RA. Systematic and integrative analysis of large gene lists using DAVID bioinformatics resources. *Nature protocols.* 2009;4(1):44-57.
3. Huang DW, Sherman BT, and Lempicki RA. Bioinformatics enrichment tools: paths toward the comprehensive functional analysis of large gene lists. *Nucleic acids research.* 2009;37(1):1-13.
4. Byrt T, Bishop J, and Carlin JB. Bias, prevalence and kappa. *Journal of clinical epidemiology.* 1993;46(5):423-9.
5. Huang DW, Sherman BT, Tan Q, Collins JR, Alvord WG, Roayaei J, Stephens R, Baseler MW, Lane HC, and Lempicki RA. The DAVID Gene Functional Classification Tool: a novel biological module-centric algorithm to functionally analyze large gene lists. *Genome biology.* 2007;8(9):R183.